

Prediction-Powered Risk Monitoring of Deployed Models for Detecting Harmful Distribution Shifts

Guangyi Zhang¹ Yunlong Cai¹ Guanding Yu¹ Osvaldo Simeone²

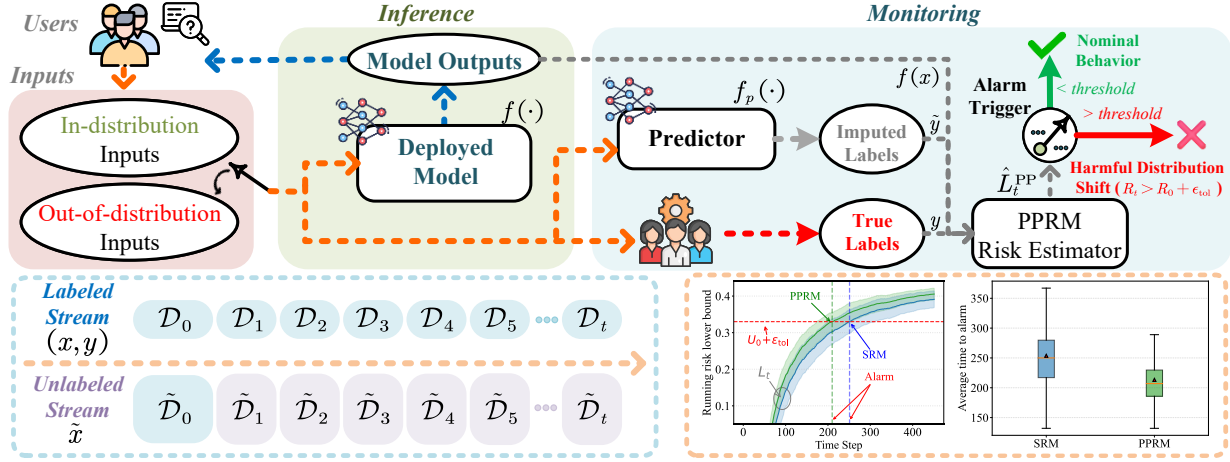


Figure 1. Over a discrete-time index, $t = 1, 2, \dots$, a deployed system is monitored to detect harmful data distribution shifts that cause the running risk \hat{R}_t to exceed the nominal risk R_0 by more than a maximum tolerated value ϵ_0 . Supervised risk monitoring (SRM) assumes access to labeled calibration dataset \mathcal{D}_t for $t = 0, 1, \dots$ (with $t = 0$ corresponding to nominal behavior) of the form (x, y) , where x is the input and y is the true label. In contrast, the proposed prediction-powered risk monitoring (PPRM) leverages both labeled data and unlabeled data $\tilde{\mathcal{D}}_1, \tilde{\mathcal{D}}_2, \dots$, including inputs \tilde{x} only, by integrating an auxiliary pre-designed function $f_p(\cdot)$, yielding synthetic labels $\tilde{y} = f_p(\tilde{x})$.

Abstract

We study the problem of monitoring model performance in dynamic environments where labeled data are limited. To this end, we propose prediction-powered risk monitoring (PPRM), a semi-supervised risk-monitoring approach based on prediction-powered inference (PPI). PPRM constructs anytime-valid lower bounds on the running risk by combining synthetic labels with a small set of true labels. Harmful shifts are detected via a threshold-based comparison with an upper bound on the nominal risk, satisfying assumption-free finite-sample guarantees in the probability of false alarm. We demonstrate the effectiveness of PPRM through extensive experiments on image classification, large language model (LLM), and telecommunications monitoring tasks.

1. Introduction

Modern machine learning models have been widely deployed in dynamic real-world environments where the underlying data distribution may shift over time (Zawalski et al., 2025). In such scenarios, systems can experience performance degradation due to factors such as changed environmental conditions (Lipton et al., 2018), as well as evolving user preferences (Guan et al., 2025). This raises concerns about reliability and safety, particularly in critical applications such as autonomous driving (Sun et al., 2025), medical diagnosis (Zeb et al., 2024), and engineering (Simeone et al., 2025). Consequently, there is a pressing need to continuously monitor the performance of deployed models.

Once a monitoring system raises an exception, the deployed machine learning model may be deemed to require retraining or substitution. Given the cost associated with such

¹College of Information Science and Electronic Engineering, Zhejiang University, Hangzhou 310027, China ²Intelligent Networked Systems Institute (INSI), Northeastern University London, E1 8PH London, U.K.. Correspondence to: Yunlong Cai <ylcai@zju.edu.cn>.

extreme measures, recent works have suggested to design sequential testing frameworks that offer formal false alarm guarantees (Podkopaev & Ramdas, 2021; I Amoukou et al., 2024; Schirmer et al., 2025). As shown in Figure 1, these methods aim to raise an alarm when the time-averaged accumulated expected risk exceeds a predefined threshold. The initial work (Podkopaev & Ramdas, 2021) introduced supervised risk monitoring (SRM), which is based on time-uniform concentration bounds obtained from labeled calibration data. Thanks to the anytime-valid properties of such bounds, SRM guarantees assumption-free false-alarm requirements.

However, labeled data from deployed models is often scarce and costly to obtain, making conventional fully supervised monitoring challenging. Based on this observation, (I Amoukou et al., 2024) introduced purely unsupervised monitoring methodologies, which do not require labels for monitoring. However, in order to provide false alarm guarantees, purely unsupervised methods require assumptions on the calibration of the deployed model, which is used to impute available labels. These assumptions are difficult to validate. Furthermore, unsupervised approaches typically require a large number of samples to achieve reliable detection, which may not be practical in many real-world settings.

To address these challenges, we propose *prediction-powered risk monitoring* (PPRM), a framework that generalizes SRM to the semi-supervised setting based on *prediction-powered inference* (PPI) (Angelopoulos et al., 2023a). As illustrated in Figure 1, PPRM assumes the availability of both labeled data and unlabeled data at each monitoring bound. Following PPI, PPRM utilizes predictions on unlabeled data as synthetic labels, while correcting the resulting bias using a small set of labeled samples. In this way, PPRM can provide risk estimates with lower variance, and thus produces tighter confidence bounds than SRM. Therefore, as shown at the bottom of Figure 1, the lower bound can exceed the threshold earlier, while also providing a similar false alarm guarantee.

We illustrate our procedure in three case studies, including image classification, large language model (LLM) monitoring via an LLM-as-a-judge (Zheng et al., 2023), and a channel equalization task in a telecommunication system (Zecchin et al., 2023).

Our main contributions are as follows:

- We propose PPRM, a semi-supervised framework for risk monitoring of deployed machine learning models that leverages both labeled and unlabeled data. The scheme applies an online procedure to adaptively adjust the reliance on unlabeled data, enabling tighter bounds without compromising statistical validity.

- We prove that PPRM provides rigorous assumption-free statistical guarantees on the probability of false alarm.
- We validate our methods through multiple case studies, including LLM monitoring via an LLM-as-a-judge, showing that PPRM achieves more accurate and timely risk monitoring compared to existing supervised and unsupervised methods.

2. Problem Formulation

In this section, we formalize the problem of monitoring model performance over time with the aim of identifying harmful distribution shifts that cause an excessive degradation in performance. We also review the benchmark approach introduced in (Podkopaev & Ramdas, 2021).

2.1. Setting and Problem Formulation

As illustrated in Figure 1, we focus on a standard multi-class classification framework, where the input domain is represented by a set $\mathcal{X} \subseteq \mathbb{R}^D$ and the output label space is $\mathcal{Y} = \{1, \dots, C\}$, with C denoting the total number of classes. We study the problem of monitoring the performance of a deployed model $f(x) \in \mathcal{O}$, while processing test data sequentially. The output space \mathcal{O} refers to the label space \mathcal{Y} or to the space of probability distributions over \mathcal{Y} , depending on whether the prediction is deterministic or probabilistic. We fix a loss function $\ell : \mathcal{O} \times \mathcal{Y} \rightarrow \mathbb{R}$, which is assumed to be bounded in the interval $[0, 1]$.

Each data point (x, y) corresponds to an independent realization from an unknown joint probability distribution over set $\mathcal{X} \times \mathcal{Y}$. *Prior* to deployment, we assume access to a *calibration dataset*, whose data points are assumed to be sampled independently and identically from a fixed *source distribution* P_0 . This distribution represents nominal conditions under which the deployed model $f(x)$ is known to perform satisfactorily. For instance, for a robotics application, calibration data may be collected in environments for which the robot has been extensively trained and validated.

At *deployment time*, test data are received *sequentially* over a discrete time index $t = 1, 2, \dots$, and are assumed to be sampled from a potentially non-stationary *test distribution*, denoted by P_t for $t = 1, 2, \dots$. No specific assumptions are imposed on the distributional shifts encoded by the sequence $\{P_t\}_{t \geq 1}$ over time. The goal is to quickly detect if the distributions P_t are sufficiently distinct from the nominal distribution P_0 to cause a harmful shift, translating into an excessive degradation in model performance.

In more detail, the calibration dataset $\mathcal{D}_0 = \{(x_{0,i}, y_{0,i})\}_{i=1}^{n_0}$ is assumed to be drawn i.i.d. from the source distribution P_0 . Furthermore, at each discrete

test time t , a dataset $\mathcal{D}_t = \{(x_{t,i}, y_{t,i})\}_{i=1}^{n_t}$ is obtained whose samples $(x_{t,i}, y_{t,i})$ are drawn i.i.d. from the test distribution P_t . The corresponding average loss under the test distribution P_t is defined as

$$R_t = \mathbb{E} [\ell(f(x_t), y_t)], \quad (1)$$

with $(x_t, y_t) \sim P_t$, for $t = 0, 1, \dots$

The quantity R_0 corresponds to the *source risk*, i.e., to the expected loss when inputs are drawn from the source distribution P_0 . As mentioned, this serves as a benchmark nominal risk, and excessive positive deviations from it signal a harmful distribution shift.

The test performance is evaluated by the *running test risk* (Podkopaev & Ramdas, 2021)

$$\bar{R}_t = \frac{1}{t} \sum_{t'=1}^t R_{t'}, \quad (2)$$

which measures the average test risk of the model across the first t test time steps. If, at some time point t^* , the running risk \bar{R}_{t^*} exceeds the baseline source risk R_0 by a pre-defined tolerance parameter $\epsilon_{\text{tol}} > 0$, i.e., if

$$\bar{R}_{t^*} > R_0 + \epsilon_{\text{tol}}, \quad (3)$$

the risk monitor should ideally raise an alarm, indicating that deployment may be stopped and retraining or fine-tuning be initiated.

Accordingly, *risk monitoring* addresses the binary hypothesis test defined by the hypotheses

$$\mathcal{H}_0 : \bar{R}_t \leq R_0 + \epsilon_{\text{tol}}, \quad \forall t \geq 1, \quad (4a)$$

$$\mathcal{H}_1 : \exists t^* \geq 1 \text{ such that } \bar{R}_{t^*} > R_0 + \epsilon_{\text{tol}}. \quad (4b)$$

The null hypothesis \mathcal{H}_0 stipulates that the running test risk never exceeds the nominal risk R_0 by more than the tolerance ϵ_{tol} , while the alternative hypothesis \mathcal{H}_1 covers cases in which the running risk exhibits a *harmful degradation*, i.e., $\bar{R}_{t^*} > R_0 + \epsilon_{\text{tol}}$ for at least one time t^* .

In practice, the nominal risks R_t , for all indices $t = 0, 1, \dots$, are not directly accessible, but they can be estimated based on the available data via the *empirical risks*

$$\hat{R}_t = \frac{1}{n_t} \sum_{i=1}^{n_t} \ell(f(x_{t,i}), y_{t,i}) \quad (5)$$

for $t = 0, 1, \dots$ Using these estimates, at each time step t , a sequential test processes the first t estimates $\hat{R}_0, \hat{R}_1, \dots, \hat{R}_t$ to output a decision

$$\Phi_t = \begin{cases} 0, & \text{continue testing,} \\ 1, & \text{reject hypothesis } \mathcal{H}_0 \text{ (alarm).} \end{cases} \quad (6)$$

Accordingly, a decision $\Phi_t = 1$ indicates that there is enough evidence to reject the null hypothesis \mathcal{H}_0 that no harmful shift has occurred, while the decision $\Phi_t = 0$ causes the test to continue operating.

The design goal for the decision rule is to control the *probability of false alarm* (PFA), i.e., the probability of producing decision $\Phi_t = 1$ when the null hypothesis \mathcal{H}_0 of no harmful shifts holds true. The PFA requirement can be formulated as the inequality

$$\mathbb{P}_{\mathcal{H}_0} (\exists t \geq 1 : \Phi_t = 1) \leq \delta, \quad (7)$$

where $\delta \in (0, 1)$ is a user-defined value, and $P_{\mathcal{H}_0}$ denotes any probability sequence P_1, P_2, \dots satisfying the condition (4a).

Besides guaranteeing the PFA condition (7), one is also interested in reducing the average time required for correctly detecting a harmful shift. Formally, since the earliest time an alarm is produced as $\min\{t \geq 1 : \Phi_t = 1\}$, the average time to alarm is defined as the expected stopping time

$$T = \mathbb{E} [\min \{t \geq 1 : \Phi_t = 1\}]. \quad (8)$$

2.2. Supervised Risk Monitoring

Given the estimated risks $\hat{R}_0, \hat{R}_1, \dots, \hat{R}_t$ in (5), the *supervised risk monitoring* (SRM) method introduced in (Podkopaev & Ramdas, 2021) constructs an upper bound U_0 on the source risk R_0 and a lower bound L_t on the running test risk \bar{R}_t as

$$U_0 = \hat{R}_0 + w_0, \quad \text{and} \quad L_t = \hat{R}_t - w_t, \quad (9)$$

where w_0 and w_t are finite-sample correction terms, and $\hat{R}_t = t^{-1} \sum_{t'=1}^t \hat{R}_{t'}$ denotes the empirical estimates of running risk.

The correction term w_0 is selected so as to ensure that the true source risk R_0 is upper bounded by U_0 with probability no smaller than $1 - \delta_S$, i.e.,

$$\mathbb{P}(R_0 \leq U_0) \geq 1 - \delta_S, \quad (10)$$

for a given probability $\delta_S \in (0, 1)$. For example, the constant w_0 can be obtained using Hoeffding's inequality as $w_0 = \sqrt{\ln(1/\delta_S)/2n_0}$, given that the loss is assumed to be bounded (Fisher & Sen, 1994; Einbinder et al., 2025).

In contrast, the constants w_t are chosen such that the sequence $\{L_t\}_{t \geq 1}$ forms an *anytime-valid* lower bound on the running test risk. Formally, this requirement is captured by the inequality

$$\mathbb{P}(\bar{R}_t \geq L_t, \forall t \geq 1) \geq 1 - \delta_T, \quad (11)$$

for some confidence level $\delta_T \in (0, 1)$. This bound can be obtained by leveraging the following lemma.

Lemma 2.1 (Theorem 4, Conjugate-mixture empirical Bernstein (CM-EB) adapted from (Howard et al., 2021)). *Consider a sequence of random variables $\{Z_t\}_{t \geq 1}$ with $Z_t \in [0, 1]$ for all $t \geq 1$. Define the time-averaged mean $\mu_t = t^{-1} \sum_{t'=1}^t \mathbb{E}[Z_{t'}]$, and the empirical mean $\hat{\mu}_t = t^{-1} \sum_{t'=1}^t Z_{t'}$. Let $\{\hat{Z}_t\}_{t \geq 1}$ be any predictable sequence with $\hat{Z}_t \in [0, 1]$, in the sense that each variable \hat{Z}_t is a function of the past variables Z_1, \dots, Z_{t-1} only. Define the function $u(V_t) = \sup \{S : \int_0^1 q(\lambda) \exp(\lambda S - \psi_E(\lambda) V_t) d\lambda < 1/\delta_T\}$ for any distribution $q(\lambda)$ on parameter λ , where $V_t = \sum_{t'=1}^t (Z_{t'} - \hat{Z}_{t'})^2$ is the cumulative prediction error, $\psi_E(\lambda) = -\log(1-\lambda) - \lambda$, and $\delta_T \in (0, 1)$ is a probability. Then, we have the inequality*

$$\mathbb{P}\left(\forall t \geq 1 : |\mu_t - \hat{\mu}_t| < \frac{u(V_t)}{t}\right) \geq 1 - 2\delta_T. \quad (12)$$

In the context of SRM, the confidence sequence (12) in Lemma 2.1 can be leveraged to obtain an anytime-valid lower confidence bound (9) with the correction term $w_t = u(V_t)/t$, and with the variance process V_t becomes $V_t = \sum_{t'=1}^t (\hat{R}_{t'} - \bar{R}_{t-1})^2$.

By combining both bounds, i.e., (10) and (11), SRM obtains the decision variable as

$$\Phi_t = \mathbb{1}[L_t > U_0 + \epsilon_{\text{tol}}], \quad (13)$$

where $\mathbb{1}[\cdot]$ is the indicator function. As shown in Figure 1, this decision rule triggers an alarm when the lower bound on the running test risk \bar{R}_t exceeds the upper bound on source risk R_0 plus the tolerance margin ϵ_{tol} . Accordingly, the average earliest detection time (8) is given by

$$T = \mathbb{E}[\min\{t \geq 1 : L_t > U_0 + \epsilon_{\text{tol}}\}]. \quad (14)$$

SRM satisfies the PFA requirement (7) as long as one chooses the probabilities in (10) and (11) as $\delta = \delta_S + \delta_T$, as formalized in the following lemma.

Lemma 2.2 (PFA Guarantee of SRM (Podkopaev & Ramdas, 2021)). *Given user-defined miscoverage levels $\delta_S, \delta_T \in (0, 1)$, satisfying the equality $\delta_S + \delta_T \in (0, 1)$, SRM provides the following guarantee on the PFA:*

$$\mathbb{P}_{\mathcal{H}_0}(\exists t \geq 1, \Phi_t = 1) \leq \delta_S + \delta_T. \quad (15)$$

3. Semi-Supervised Risk Monitoring

In many real-world deployments, acquiring labeled feedback is costly and time-consuming, while unlabeled test data are abundant and arrive continuously. As shown in Figure 1, this motivates a semi-supervised paradigm where the risk monitor can leverage a small set of labeled samples, together with a larger pool of unlabeled observations. To

address this setting, in this section, we propose a generalization of SRM (Podkopaev & Ramdas, 2021) referred to as *prediction-powered semi-supervised risk monitoring* (PPRM), that can leverage both labeled and unlabeled data.

3.1. Prediction-Powered Risk Estimates

As shown in Figure 1, at each time step $t = 1, 2, \dots$, the monitor observes a labeled batch $\mathcal{D}_t = \{(x_{t,i}, y_{t,i})\}_{i=1}^{n_t}$, as for SRM, along with an unlabeled batch $\tilde{\mathcal{D}}_t = \{\tilde{x}_{t,i}\}_{i=n_t+1}^{n_t+N_t}$ of N_t inputs with no associated labels. The main challenge in this setting lies in how to efficiently combine the labeled and unlabeled streams while satisfying the PFA condition (7). We emphasize that, unlike (Schirmer et al., 2025; I Amoukou et al., 2024), we assume that the number of labeled data points, n_t , is strictly positive. As we will see, this allows us to avoid the technical assumptions required in (Schirmer et al., 2025) about the error rates of the models used to generate synthetic labels for the unlabeled data.

PPRM incorporates PPI-based estimates of the risks (Angelopoulos et al., 2023a) into the SRM framework. Through PPI, PPRM constructs unbiased empirical estimates of the risks by: (i) using a predictive model $f_p(\cdot)$ to generate synthetic labels for the unlabeled portion of the data; and then (ii) correcting for the systematic bias caused by the synthetic labels via calibration using the labeled samples. The labeling model $f_p(\cdot)$ may be, for instance, a general-purpose expert, such as an LLM, or possibly the deployed model $f(\cdot)$ itself. As anticipated, unlike (Schirmer et al., 2025), we do not make any assumptions on the quality of the model $f_p(\cdot)$.

Write as $\tilde{y}_{t,i}$ the synthetic labels for the unlabeled input $\tilde{x}_{t,i}$, i.e.,

$$\tilde{y}_{t,i} = \arg \max_c f_p(\tilde{x}_{t,i}) [c], \quad (16)$$

where $f_p(\cdot)[c]$ denotes the predicted probability assigned to class c by the predictive model $f_p(\cdot)$. Using PPI, the source risk R_0 is estimated as

$$\begin{aligned} \hat{R}_0^{\text{PP}} &= \underbrace{\frac{\eta_0}{N_0} \sum_{j=n_0+1}^{n_0+N_0} \ell(f_0(\tilde{x}_{0,j}), \tilde{y}_{0,j})}_{\hat{R}_0^{\text{U}}} \\ &\quad + \underbrace{\frac{1}{n_0} \sum_{i=1}^{n_0} \ell(f_0(x_{0,i}), y_{0,i}) - \frac{\eta_0}{n_0} \sum_{i=1}^{n_0} \ell(f_0(x_{0,i}), \tilde{y}_{0,i})}_{\hat{R}_0^{\text{rect}}} \end{aligned} \quad (17)$$

where $\eta_0 \geq 0$ is a hyperparameter that controls the reliance of the estimate on the unlabeled data (Angelopoulos et al., 2023b). The first term \hat{R}_0^{U} in (17) is the empirical risk evaluated only with the unlabeled synthetic data, while the second term \hat{R}_0^{rect} estimates the bias introduced by the imputation. As proved in (Angelopoulos et al., 2023a), using PPI++,

the empirical estimate \hat{R}_0^{PP} is unbiased, in the sense that $\mathbb{E}[\hat{R}_0^{\text{PP}}] = R_0$, for any choice of hyperparameter $\eta_0 \geq 0$.

In a similar way, the running test risk \bar{R}_t is estimated as

$$\begin{aligned} \hat{R}_t^{\text{PP}} = & \frac{1}{t} \sum_{t'=1}^t \left[\underbrace{\frac{\eta_{t'}}{N_{t'}} \sum_{j=n_{t'}+1}^{n_{t'}+N_{t'}} \ell(f(\tilde{x}_{t',j}), \tilde{y}_{t',j})}_{\hat{R}_{t'}^{\text{U}}} \right. \\ & \left. + \underbrace{\frac{1}{n_{t'}} \sum_{i=1}^{n_{t'}} \ell(f(x_{t',i}), y_{t',i}) - \frac{\eta_{t'}}{n_{t'}} \sum_{i=1}^{n_{t'}} \ell(f(x_{t',i}), \tilde{y}_{t',i})}_{\hat{R}_{t'}^{\text{rect}}} \right], \end{aligned} \quad (18)$$

using both labeled and unlabeled data, where η_t plays the same role as in (17). Furthermore, as in (17), the first term \hat{R}_t^{U} in (18) denotes the empirical risk evaluated only with the unlabeled synthetic data at time step t , while the second term \hat{R}_t^{rect} estimates the bias introduced by the imputation. We write

$$\hat{R}_t^{\text{PP}} = \hat{R}_t^{\text{U}} + \hat{R}_t^{\text{rect}} \quad (19)$$

for the contribution to the estimate (18) corresponding to each time step t .

Lemma 3.1 (Unbiasedness of PPRM). *Assume that the hyperparameters $\{\eta_t\}_{t \geq 1}$ form a predictable sequence, in the sense that each hyperparameter η_t is a function only of the data $\{\mathcal{D}_{t'}, \tilde{\mathcal{D}}_{t'}, \{\tilde{y}_{t',i}\}_{i=1}^{n_{t'}+N_{t'}}\}_{t'=1}^{t-1}$ observed strictly before time t . Then, the quantity (18) is an unbiased estimate of the corresponding true risk, i.e.,*

$$\mathbb{E}[\hat{R}_t^{\text{PP}}] = \bar{R}_t. \quad (20)$$

The proof can be found in Appendix A.1.

3.2. Upper and Lower PPRM Bounds

As in SRM, PPRM obtains an upper bound U_0^{PP} on the source risk, as well as a lower confidence bound L_t^{PP} for $t = 1, 2, \dots$, which are denoted respectively by

$$U_0^{\text{PP}} = \hat{R}_0^{\text{PP}} + w_0^{\text{PP}} \quad \text{and} \quad L_t^{\text{PP}} = \hat{R}_t^{\text{PP}} - w_t^{\text{PP}}. \quad (21)$$

The correction term w_0^{PP} is designed to ensure the inequality $\mathbb{P}(R_0 \leq U_0^{\text{PP}}) \geq 1 - \delta_S$, and we adopt here the betting-based method from (Einbinder et al., 2025). Further details are provided in Appendix A.2. To compute the correction terms w_t^{PP} , we apply the confidence sequence bound in Lemma 2.1 to the PPI-based risk estimates.

To this end, since the prediction-powered estimates \hat{R}_t^{PP} take values in the interval $[-\eta_t, \eta_t + 1]$, we first apply an affine normalization $g_a(\cdot)$, i.e., $g_a(\ell) = (\ell + \eta_{\max}) / (1 + 2\eta_{\max})$, to the loss function ℓ so that each estimate \hat{R}_t^{PP} lies in the range $[0, 1]$, where η_{\max} is the maximum permitted value for η_t .

With the rescaled loss, the correction term w_t^{PP} is given by $w_t^{\text{PP}} = u(V_t^{\text{PP}})/t$, with $u(V_t^{\text{PP}}) = \sup\{S : \int_0^1 q(\lambda) \exp(\lambda S - \psi_E(\lambda)V_t^{\text{PP}}) d\lambda < 1/\delta_T\}$, where

$$V_t^{\text{PP}} = \sum_{t'=1}^t (\hat{R}_{t'}^{\text{PP}} - \hat{R}_{t'-1}^{\text{PP}})^2. \quad (22)$$

The term V_t^{PP} in (22) is the cumulative squared prediction error for the estimate $\hat{R}_{t'}^{\text{PP}}$ in (19) when using the corresponding time-average up to time $t-1$, i.e., $\hat{R}_{t'-1}^{\text{PP}}$ in (18), as the prediction.

PPRM then applies the decision rule as

$$\Phi_t^{\text{PP}} = \mathbb{1}[L_t^{\text{PP}} > U_0^{\text{PP}} + \epsilon_{\text{tol}}]. \quad (23)$$

Following the same argument as Lemma 2.2, we have the following result.

Theorem 3.2 (PFA Guarantee of PPRM). *Given user-defined miscoverage levels $\delta_S, \delta_T \in (0, 1)$, satisfying the condition $\delta_S + \delta_T \in (0, 1)$, let $\{\eta_t\}_{t \geq 1}$ be any predictable sequence, as defined in Lemma 3.1. Then, PPRM provides the following guarantee on the PFA:*

$$\mathbb{P}_{\mathcal{H}_0}(\exists t \geq 1 : \Phi_t^{\text{PP}} = 1) \leq \delta_S + \delta_T. \quad (24)$$

To prove this result, it suffices to note that, as long as the sequence $\{\eta_t\}_{t \geq 1}$ is predictable, the prediction-powered risk estimates (17) and (18) are unbiased by Lemma 3.1. The proof then follows directly from Lemma 2.2.

3.3. Optimizing the Reliance on Unlabeled Data

The prediction-powered risk estimate \hat{R}_t^{PP} relies on the unlabeled data to an extent that depends on the hyperparameter η_t by leveraging the result in Lemma 3.1, which allows η_t to be a function of past data up to time $t-1$.

To this end, we propose to minimize the average value of the prediction error V_t^{PP} in (22), which determines the tightness of the lower bound L_t^{PP} in (21). A tighter bound ensures that, when the alternative hypothesis (4b) holds, the PPRM test (23) signals a harmful degradation, setting $\Phi_t^{\text{PP}} = 1$, at an earlier time t .

Lemma 3.3 (Optimal Choice of η_t for Variance Reduction). *Let $\hat{R}_t^{\text{PP}}(\eta_t)$ denote the prediction-powered empirical risk (19) at time t , which is parameterized by the hyperparameter η_t . The value of hyperparameter η_t that minimizes the one-step variance, i.e.,*

$$\eta_t^* = \arg \min_{\eta_t \geq 0} \mathbb{E}[(\hat{R}_t^{\text{PP}}(\eta_t) - \hat{R}_{t-1}^{\text{PP}})^2], \quad (25)$$

is given by

$$\eta_t^* = \frac{\text{Cov}(u_t, \tilde{u}_t)}{(1 + \frac{n_t}{N_t}) \text{Var}(\tilde{u}_t)}, \quad (26)$$

where $u_t = \ell(f(x_t), y_t)$ denotes the true loss, $\tilde{u}_t = \ell(f(\tilde{x}_t), f_p(\tilde{x}_t))$ denotes the loss obtained with the predictor $f_p(\cdot)$, $\text{Var}(\cdot)$ is the variance operator, and $\text{Cov}(\cdot)$ denotes covariance.

The proof of this result, which follows in a manner similar to (Angelopoulos et al., 2023b), can be found in Appendix A.3.

The hyperparameter η_t^* in (26) depends on the true data distribution, which is unknown. Thus, we propose to estimate it using the data up to time step $t-1$ using a sliding-window approach with fixed window size L . This produces a predictable sequence $\{\eta_t\}_{t \geq 1}$, satisfying the assumption of Theorem 3.2. Specifically, we consider the following plug-in estimator

$$\eta_t = \frac{\widehat{\text{Cov}}_{\mathcal{H}_{t-1}}(u, \tilde{u})}{\left(1 + \frac{|\mathcal{H}_{t-1}|}{|\tilde{\mathcal{H}}_{t-1}|}\right) \widehat{\text{Var}}_{\tilde{\mathcal{H}}_{t-1}}(\tilde{u})}, \quad (27)$$

where $\widehat{\text{Cov}}_{\mathcal{H}_{t-1}}(u, \tilde{u})$ and $\widehat{\text{Var}}_{\tilde{\mathcal{H}}_{t-1}}(\tilde{u})$ denote the empirical estimates using the data

$$\mathcal{H}_{t-1} = \bigcup_{t'=t-L}^{t-1} \mathcal{D}_{t'}, \quad \text{and} \quad \tilde{\mathcal{H}}_{t-1} = \bigcup_{t'=t-L}^{t-1} \tilde{\mathcal{D}}_{t'}, \quad (28)$$

with $|\mathcal{H}_{t-1}|$ and $|\tilde{\mathcal{H}}_{t-1}|$ denoting the total numbers of historical labeled and unlabeled samples available before time t , respectively.

4. Related Works

Sequential Testing-Based Risk Monitoring: SRM was introduced by (Podkopaev & Ramdas, 2021) to tackle the problem of detecting harmful distribution shifts in a sequential setting. SRM builds confidence bounds for model risk using labeled calibration data (Podkopaev & Ramdas, 2021) and incoming test data, and provides time-uniform guarantees on false alarm control. Subsequently, I Amoukou et al. extended this line of work to the unlabeled production-data setting, while Schirmer et al. further explored scenarios involving test-time adaptation models without access to labels. Related approaches by (Bar et al., 2024) and (Vovk et al., 2021) focus on identifying changes in certain statistical properties. However, such changes do not necessarily indicate harmful deviations.

Beyond tracking running risk, several studies have examined the instantaneous true risk with similar false-alarm guarantees (Xu et al., 2024; Zecchin et al., 2024; Timans et al., 2025; Shekhar & Ramdas, 2023; Vovk & Wang, 2021). These methods are built around the testing-by-betting framework (Ramdas & Wang, 2025). Compared with our work, they target different hypotheses and operate under distinct experimental setups.

Prediction-Powered Inference: In many practical settings, models can access large pools of unlabeled data but only a limited amount of costly ground-truth labels. PPI was introduced to make use of predictions from an auxiliary model to facilitate statistical inference. Its key idea is to construct prediction-powered estimators that remain unbiased for the target risk, while using predictive information to reduce variance. The framework has since been extended in several directions, including robust PPI++ (Angelopoulos et al., 2023b), local PPI (Gu & Xia, 2024), anytime-valid PPI (Kilian et al., 2025), active PPI (Zrnic & Emmanuel, 2024), and FAB-PPI (Cortinovis & Caron, 2025). More recently, (Csillag et al., 2025) introduced prediction-powered e-values (Shafer & Vovk, 2019) for sequential change-point detection (Shekhar & Ramdas, 2023; Shin et al., 2022). Their approach also builds on the testing-by-betting paradigm (Ramdas & Wang, 2025), and therefore differs from our proposed PPRM both in the hypothesis being tested and in the experimental setup.

LLM Performance Evaluation: Selecting an appropriate model from a number of candidates requires reliable estimates of each model’s performance. Traditional evaluation methods depend on deploying models and gathering empirical evidence through real-world testing, which is often expensive to deploy. To mitigate this burden, recent studies have investigated autoevaluation techniques that automate assessment using synthetic data or automated tools, thereby reducing the need for human involvement (Chaganty et al., 2018; Zheng et al., 2023). PPI has also been applied to improve the efficiency of model evaluation (Fisch et al., 2024; Park et al., 2025; Einbinder et al., 2025). Nonetheless, the problem of monitoring a deployed model using PPI has not been explored.

5. Experiments

In this section, we present two case studies, including image classification and LLM monitoring, with one additional telecommunication task being presented in the appendix.

Baselines We compare PPRM to several baseline monitors:

- **Ideal PPRM:** This is an idealized case where PPRM has full access to the true labels of both labeled dataset \mathcal{D}_t and unlabeled dataset $\tilde{\mathcal{D}}_t$. This produces the performance upper bound corresponding to full label access.
- **SRM (Podkopaev & Ramdas, 2021):** As discussed in Section 2.2, SRM uses only the labeled data \mathcal{D}_t .
- **Unsupervised risk monitoring (URM) (Schirmer et al., 2025):** This scheme uses only unlabeled data and is reviewed in Appendix B.

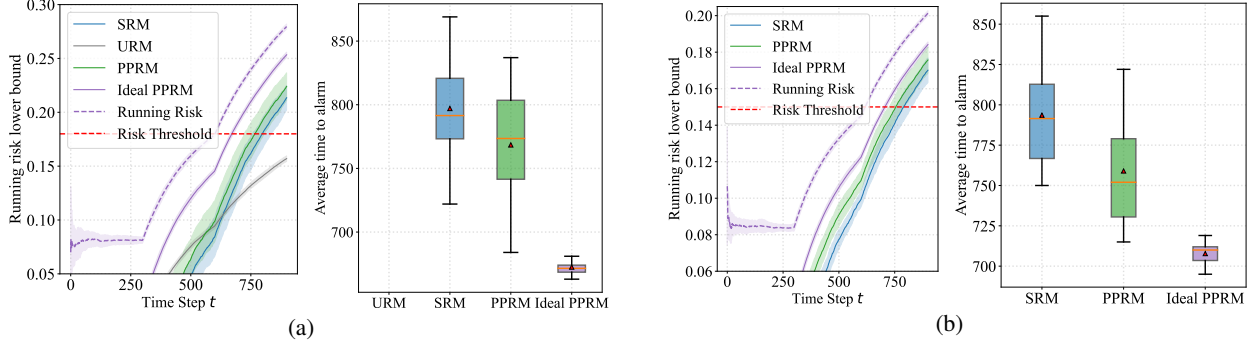


Figure 2. Risk estimates as a function of time t and average time to alarm for an image classification task under increasing shift severity: (a) binary loss monitored with an external predictor; (b) squared loss monitored using labels produced by the deployed model itself.

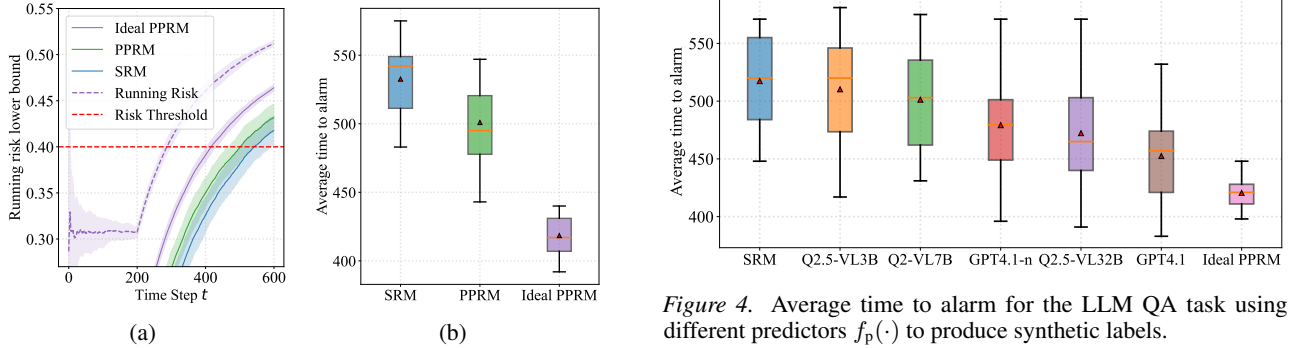


Figure 3. Performance for the LLM QA task under prompt shifts introduced as time $t = 200$: (a) Running risk lower bounds, using Qwen2-VL-7B as the predictive model for imputation; (b) Average time to alarm.

We focus on binary 0–1 loss and squared loss. If not specified otherwise, we set $\delta = \delta_S + \delta_T = 0.25$, allocating most of the budget to controlling the test risk, i.e., $\delta_T = 0.2$ and $\delta_S = 0.05$. We set $\eta_0 = 1$ in (17), and the window length L to obtain η_t (27) is set to 60. The numbers of labeled data samples and unlabeled data samples at each time step are set to 1 and 15. To compute all the lower bounds of the running risk, we adopt the CM-EB method reviewed in Lemma 2.1. In all figures, the error bar represents the full range across all runs.

5.1. Sequential Risk Monitoring on Image Data

5.1.1. PROBLEM FORMULATION

We first consider the task of risk monitoring in the vision domain, replicating the setting of (Schirmer et al., 2025), where the CIFAR10-C (Hendrycks & Dietterich, 2019) dataset was considered. Accordingly, the test-time distribution is obtained by applying Gaussian noise with three levels of severity to the image distribution corresponding to the nominal condition. We monitor the performance of

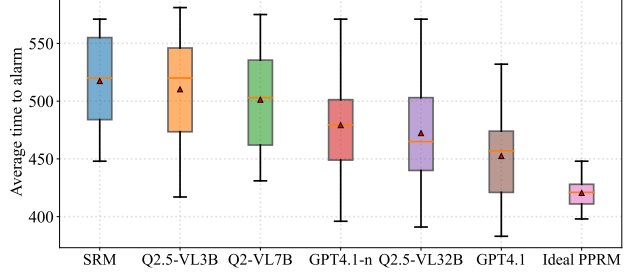


Figure 4. Average time to alarm for the LLM QA task using different predictors $f_p(\cdot)$ to produce synthetic labels.

a ResNet-32 model (He et al., 2016) trained on nominal data. To generate synthetic labels for unlabeled samples, we employ the ResNet-1201 trained on the same dataset.

5.1.2. RESULTS

Monitoring with Drifting Data Distribution: To simulate an increasing test risk, we gradually increase the severity level of Gaussian noise corruption from nominal data, i.e., severity level 0, up to severity level 2. Figure 2(a) shows the results of the estimated test risk and of the alarm decisions. As the corruption intensifies, the true risk exceeds the safe threshold at time $t = 600$, PPRM raises an alarm at around time $t = 760$, whereas SRM reacts more slowly, at around time $t = 800$ due to high estimation variance, and URM fails to trigger an alarm within the considered time period.

Monitoring with Self-Synthetic Strategy: The proposed PPRM can also be applied when the model itself is used to provide label surrogates for the unlabeled data. For this setting, focusing on C -class classification, we consider the squared loss between labels and model confidence levels, i.e., $\ell(f(x), y) = \frac{1}{2} \sum_{c=1}^C (f(x)_c - \mathbb{1}[y = c])^2$, as the loss function. This squared loss corresponds to the Brier score when averaged across samples, and it was also adopted in (Schirmer et al., 2025).

As seen in Figure 2(b), even without an additional predictor, PPRM can reduce the time to alarm by making use of the model’s intrinsic confidence signals. In particular, an alarm is raised at around time $t = 760$, while SRM requires $t = 790$ time steps.

5.2. Monitoring an LLM with Limited Human-Labeled Data

5.2.1. PROBLEM FORMULATION

We now focus on an LLM deployed to address *question-answering* (QA) tasks. We draw from several established benchmarks, including MMLU (Hendrycks et al., 2021), CMExam (Liu et al., 2023), CommonsenseQA (Talmor et al., 2019), Social-IQA, and PubMedQA (Jin et al., 2019). We use Qwen2-VL-2B (Wang et al., 2024) as the deployed model whose performance we aim to monitor. For the monitoring LLM, we experiment with a diverse set of both open-source and closed-source models.

5.2.2. RESULTS

To simulate an environment in which risk increases over time, starting from time $t = 200$, we introduce more complex prompts that the deployed model cannot answer correctly, causing the model’s performance to deteriorate. These complex prompts are obtained by retaining cases where a different model, namely Qwen2.5-VL-7B, fails to produce correct answers.

Monitoring with Drifting Data Distribution: As shown in Figure 3, confirming the results in the previous example, PPRM significantly reduces the average time to alarm. In particular, while the true risk exceeds the allowed level at $t = 280$, PPRM raises an alarm at around time $t = 500$, while SRM raises an alarm at around time $t = 530$.

We then further assess how the accuracy of the LLM predictor affects performance by testing a range of different labeling models, namely Qwen2.5-VL-3B (abbreviated as “Q2.5-VL3B”), Qwen2.5-VL-32B (abbreviated as “Q2.5-VL32B”) (Bai et al., 2025), Qwen2-VL-7B (abbreviated as “Q2-VL7B”) (Wang et al., 2024), GPT4.1-nano (abbreviated as “GPT4.1-n”), and GPT4.1 (Achiam et al., 2023).

The results are shown in Figure 4 by ordering the models from least to most powerful. As seen in the figure, when the LLM predictor exhibits higher accuracy, i.e., for larger models, the estimated accuracy of synthetic labels is increased, leading to a tighter bound on the monitored model’s running risk, and consequently to a lower average time to alarm.

Effect of Hyperparameter Optimization: Table 1 reports the average time to alarm for PPRM with a fixed hyperparameter $\eta_t = 1$ and with an adaptive hyperparameter

Table 1. Average time to alarm for PPRM with a fixed or an adaptive hyperparameter η_t .

<i>Predictor</i> $f_p(\cdot)$	<i>PPRM (Fixed)</i>	<i>PPRM (Adaptive)</i>
Q2.5-VL-3B	527.80	508.83
Q2-VL-7B	519.08	498.31
GPT-4.1-n	491.80	476.98
Q2.5-VL-32B	486.22	471.85
GPT-4.1	460.69	449.88

η_t in (27). The two PPRM variants are identified as “PPRM (Fixed)” and “PPRM (Adaptive)”, respectively. We consider the different imputing predictors $f_p(\cdot)$ considered in Figure 4. The table illustrates the benefits of the adaptive selection, particularly for small- and medium-sized predictors. For example, for the Qwen2-VL-7B model, the average time to alarm decreases from around 519 to around 498 thanks to adaptive hyperparameter selection. It is also observed that, as the predictor becomes stronger, the performance gap between PPRM with fixed and adaptive hyperparameters gradually narrows. This demonstrates that adaptive hyperparameter selection, determining the reliance on unlabeled data, is particularly important for less effective imputation models.

6. Conclusion

In this work, we have presented a novel framework for sequential semi-supervised risk monitoring, extending classical supervised approaches to leverage both labeled and unlabeled data. By integrating PPI, our method, termed PPRM, provided unbiased estimates of the running test risk, while maintaining rigorous statistical guarantees on the false-alarm rate. Through extensive experiments on three tasks, we have demonstrated that the proposed approach consistently achieved timely detection of harmful distribution shifts and outperformed purely supervised or unsupervised baselines. Future work may consider methods that integrate PPRM with unsupervised techniques such as test-time adaptation. Other interesting research directions include applications to engineering problems, e.g., in robotics.

Impact Statement

This paper presents work whose goal is to advance the field of machine learning. The impact of this paper may be more pronounced in engineering applications, such as telecommunication and robotics.

References

Achiam, J., Adler, S., Agarwal, S., Ahmad, L., Akkaya, I., Aleman, F. L., Almeida, D., Altenschmidt, J., Altman, S.,

Anadkat, S., et al. GPT-4 technical report. *arXiv preprint arXiv:2303.08774*, 2023.

Angelopoulos, A. N., Bates, S., Fannjiang, C., Jordan, M. I., and Zrnic, T. Prediction-powered inference. *Science*, 382(6671):669–674, 2023a.

Angelopoulos, A. N., Duchi, J. C., and Zrnic, T. PPI++: Efficient prediction-powered inference. *arXiv preprint arXiv:2311.01453*, 2023b.

Bai, S., Chen, K., Liu, X., Wang, J., Ge, W., Song, S., Dang, K., Wang, P., Wang, S., Tang, J., et al. Qwen2.5-VL technical report. *arXiv preprint arXiv:2502.13923*, 2025.

Bar, Y., Shaer, S., and Romano, Y. Protected test-time adaptation via online entropy matching: A betting approach. In *Advances in Neural Information Processing Systems*, volume 37, pp. 85467–85499, 2024.

Chaganty, A. T., Mussman, S., and Liang, P. The price of debiasing automatic metrics in natural language evaluation. *arXiv preprint arXiv:1807.02202*, 2018.

Cortinovis, S. and Caron, F. FAB-PPI: Frequentist, assisted by bayes, prediction-powered inference. In *Proceedings of the International Conference on Machine Learning (ICML)*, 2025.

Csillag, D., Struchiner, C. J., and Goedert, G. T. Prediction-powered e-values. *arXiv preprint arXiv:2502.04294*, 2025.

Dietrich, F. A., Ivanov, T., and Utschick, W. Estimation of channel and noise correlations for MIMO channel estimation. In *Proc. International ITG Workshop on Smart Antennas*, Ulm, Germany, March 2006.

Einbinder, B.-S., Ringel, L., and Romano, Y. Semi-supervised risk control via prediction-powered inference. *IEEE Transactions on Pattern Analysis and Machine Intelligence*, 47(12):11080–11090, 2025.

Fisch, A., Maynez, J., Hofer, R., Dhingra, B., Globerson, A., and Cohen, W. W. Stratified prediction-powered inference for effective hybrid evaluation of language models. *Advances in Neural Information Processing Systems*, 37: 111489–111514, 2024.

Fisher, N. and Sen, P. Probability inequalities for sums of bounded random variables. In *The Collected Works of Wassily Hoeffding*, pp. 631–634. Springer, 1994.

Gu, Y. and Xia, D. Local prediction-powered inference. *arXiv preprint arXiv:2409.18321*, 2024.

Guan, H., Bates, D., and Zhou, L. Keeping medical AI healthy: A review of detection and correction methods for system degradation. *arXiv preprint arXiv:2506.17442*, 2025.

He, K., Zhang, X., Ren, S., and Sun, J. Deep residual learning for image recognition. In *Proceedings of the IEEE Conference on Computer Vision and Pattern Recognition*, pp. 770–778, 2016.

Hendrycks, D. and Dietterich, T. Benchmarking neural network robustness to common corruptions and perturbations. In *International Conference on Learning Representations*, 2019.

Hendrycks, D., Burns, C., Basart, S., Zou, A., Mazeika, M., Song, D., and Steinhardt, J. Measuring massive multitask language understanding. In *International Conference on Learning Representations*, 2021.

Howard, S. R., Ramdas, A., McAuliffe, J., and Sekhon, J. Time-uniform, nonparametric, nonasymptotic confidence sequences. *The Annals of Statistics*, 49(2):1055–1080, April 2021.

I Amoukou, S., Bewley, T., Mishra, S., Lecue, F., Magazzini, D., and Veloso, M. Sequential harmful shift detection without labels. In *Advances in Neural Information Processing Systems*, volume 37, pp. 129279–129302, 2024.

Jin, Q., Dhingra, B., Liu, Z., Cohen, W., and Lu, X. Pubmedqa: A dataset for biomedical research question answering. In *Proceedings of the 2019 conference on empirical methods in natural language processing and the 9th international joint conference on natural language processing (EMNLP-IJCNLP)*, pp. 2567–2577, 2019.

Kilian, V., Cortinovis, S., and Caron, F. Anytime-valid, bayes-assisted, prediction-powered inference. *arXiv preprint arXiv:2505.18000*, 2025.

Lipton, Z., Wang, Y.-X., and Smola, A. Detecting and correcting for label shift with black box predictors. In *International conference on machine learning*, pp. 3122–3130. PMLR, 2018.

Liu, J., Zhou, P., Hua, Y., Chong, D., Tian, Z., Liu, A., Wang, H., You, C., Guo, Z., Zhu, L., et al. Benchmarking large language models on CMExam—a comprehensive Chinese medical exam dataset. *arXiv preprint arXiv:2306.03030*, 2023.

Park, S., Zecchin, M., and Simeone, O. Adaptive prediction-powered autoeval with reliability and efficiency guarantees. *arXiv preprint arXiv:2505.18659*, 2025.

Podkopaev, A. and Ramdas, A. Tracking the risk of a deployed model and detecting harmful distribution shifts. *arXiv preprint arXiv:2110.06177*, 2021.

Ramdas, A. and Wang, R. Hypothesis testing with e-values. *Foundations and Trends® in Statistics*, 1(1-2):1–390, 2025.

Schirmer, M., Jazbec, M., Naesseth, C. A., and Nalisnick, E. Monitoring risks in test-time adaptation. *arXiv preprint arXiv:2507.08721*, 2025. URL <https://arxiv.org/abs/2507.08721>.

Sellergren, A., Kazemzadeh, S., Jaroensri, T., Kiraly, A., Traverse, M., Kohlberger, T., Xu, S., Jamil, F., Hughes, C., Lau, C., et al. Medgemma technical report. *arXiv preprint arXiv:2507.05201*, 2025.

Shafer, G. and Vovk, V. *Game-Theoretic Foundations for Probability and Finance*. Wiley Series in Probability and Statistics. John Wiley & Sons, Hoboken, NJ, 2019.

Shekhar, S. and Ramdas, A. Sequential changepoint detection via backward confidence sequences. In *International Conference on Machine Learning*, pp. 30908–30930. PMLR, 2023.

Shin, J., Ramdas, A., and Rinaldo, A. E-detectors: A non-parametric framework for sequential change detection. *arXiv preprint arXiv:2203.03532*, 2022.

Simeone, O., Park, S., and Zecchin, M. Conformal calibration: Ensuring the reliability of black-box AI in wireless systems. *arXiv preprint arXiv:2504.09310*, 2025.

Sun, W., Lin, X., Shi, Y., Zhang, C., Wu, H., and Zheng, S. Sparsedrive: End-to-end autonomous driving via sparse scene representation. In *2025 IEEE International Conference on Robotics and Automation*, pp. 8795–8801, 2025.

Talmor, A., Herzig, J., Lourie, N., and Berant, J. Commonsenseqa: A question answering challenge targeting commonsense knowledge. In *Proceedings of the 2019 Conference of the North American Chapter of the Association for Computational Linguistics: Human Language Technologies, Volume 1 (Long and Short Papers)*, pp. 4149–4158, 2019.

Timans, A., Verma, R., Nalisnick, E., and Naesseth, C. A. On continuous monitoring of risk violations under unknown shift. *arXiv preprint arXiv:2506.16416*, 2025.

Vovk, V. and Wang, R. E-values: Calibration, combination and applications. *The Annals of Statistics*, 49(3):1736–1754, 2021.

Vovk, V., Petej, I., Nouretdinov, I., Ahlberg, E., Carlsson, L., and Gammerman, A. Retrain or not retrain: Conformal test martingales for change-point detection. In *Conformal and Probabilistic Prediction and Applications*, pp. 191–210. PMLR, 2021.

Waudby-Smith, I. and Ramdas, A. Estimating means of bounded random variables by betting. *Journal of the Royal Statistical Society: Series B (Statistical Methodology)*, 86(1):1–27, 2024.

Xu, Z., Karampatziakis, N., and Mineiro, P. Active, anytime-valid risk controlling prediction sets. In *Advances in Neural Information Processing Systems*, volume 37, pp. 60110–60132, 2024.

Zawalski, M., Chen, W., Pertsch, K., Mees, O., Finn, C., and Levine, S. Robotic control via embodied chain-of-thought reasoning. *arXiv preprint arXiv:2407.08693*, 2025.

Zeb, S., Nizamullah, F., Abbasi, N., and Fahad, M. AI in healthcare: revolutionizing diagnosis and therapy. *International Journal of Multidisciplinary Sciences and Arts*, 3(3):118–128, 2024.

Zecchin, M., Park, S., Simeone, O., Kountouris, M., and Gesbert, D. Robust bayesian learning for reliable wireless ai: Framework and applications. *IEEE Transactions on Cognitive Communications and Networking*, 9(4):897–912, 2023.

Zecchin, M., Park, S., and Simeone, O. Adaptive learn-then-test: Statistically valid and efficient hyperparameter selection. *arXiv preprint arXiv:2409.15844*, 2024.

Zheng, L., Chiang, W.-L., Sheng, Y., Zhuang, S., Wu, Z., Zhuang, Y., Lin, Z., Li, Z., Li, D., Xing, E., et al. Judging LLM-as-a-judge with MT-bench and chatbot arena. In *Advances in neural information processing systems*, volume 36, pp. 46595–46623, 2023.

Zrnic, T. and Emmanuel, J. C. Active statistical inference. In *International Conference on Machine Learning (ICML)*, pp. 62993–63010, 2024.

Wang, P., Bai, S., Tan, S., Wang, S., Fan, Z., et al. Qwen2-VL: Enhancing vision-language model’s perception of the world at any resolution. *arXiv preprint arXiv:2409.12191*, 2024.

A. Proofs and Analysis

A.1. Proof of Lemma 3.1

We aim to show the equality $\mathbb{E}[\hat{R}_t^{\text{PP}}] = \bar{R}_t = t^{-1} \sum_{t'=1}^t R_{t'}$, where $R_{t'} = \mathbb{E}[\ell(f(x_{t'}), y_{t'})]$. Recall that we have

$$\begin{aligned}\hat{R}_t^{\text{PP}} &= \frac{1}{t} \sum_{t'=1}^t \left[\hat{R}_{t'}^{\text{U}} + \hat{R}_{t'}^{\text{rect}} \right] \\ &= \frac{1}{t} \sum_{t'=1}^t \left[\frac{\eta_{t'}}{N_{t'}} \sum_{j=n_{t'}+1}^{n_{t'}+N_{t'}} \ell(f(\tilde{x}_{t',j}), \tilde{y}_{t',j}) + \frac{1}{n_{t'}} \sum_{i=1}^{n_{t'}} \ell(f(x_{t',i}), y_{t',i}) - \frac{\eta_{t'}}{n_{t'}} \sum_{i=1}^{n_{t'}} \ell(f(x_{t',i}), \tilde{y}_{t',i}) \right].\end{aligned}\quad (29)$$

By linearity of expectation, we have

$$\mathbb{E}[\hat{R}_t^{\text{PP}}] = \frac{1}{t} \sum_{t'=1}^t \mathbb{E}[\hat{R}_{t'}^{\text{U}} + \hat{R}_{t'}^{\text{rect}}]. \quad (30)$$

For each term, we further have

$$\mathbb{E}[\hat{R}_t^{\text{U}} + \hat{R}_t^{\text{rect}}] = \mathbb{E}_{\eta_t}[\mathbb{E}[\hat{R}_t^{\text{U}} + \hat{R}_t^{\text{rect}} | \eta_t]]. \quad (31)$$

Since the hyperparameter η_t is only a function of data observed at times $t' = 1, \dots, t-1$, it is independent of the data observed as time t , and we have

$$\begin{aligned}\mathbb{E}[\hat{R}_t^{\text{U}} + \hat{R}_t^{\text{rect}} | \eta_t] &= \eta_t \cdot \mathbb{E}[\ell(f(\tilde{x}_t), \tilde{y}_t)] + \mathbb{E}[\ell(f(x_t), y_t) - \eta_t \cdot \ell(f(x_t), \tilde{y}_t)] \\ &= \mathbb{E}[\ell(f(x_t), y_t)] = R_t.\end{aligned}\quad (32)$$

Then, we have $\mathbb{E}[\hat{R}_t^{\text{U}} + \hat{R}_t^{\text{rect}}] = \mathbb{E}_{\eta_t}[R_t] = R_t$. Therefore, the equality $\mathbb{E}[\hat{R}_t^{\text{PP}}] = t^{-1} \sum_{t'=1}^t R_{t'} = \bar{R}_t$ holds. This completes the proof.

A.2. Source Upper Bound

The prediction-powered risk estimator on the source domain is given by (17), i.e.,

$$\hat{R}_0^{\text{PP}} = \underbrace{\frac{1}{N_0} \sum_{j=n_0+1}^{n_0+N_0} \ell(f_0(\tilde{x}_{0,j}), \tilde{y}_{0,j})}_{\hat{R}_0^{\text{U}}} + \underbrace{\frac{1}{n_0} \sum_{i=1}^{n_0} \ell(f_0(x_{0,i}), y_{0,i}) - \frac{1}{n_0} \sum_{i=1}^{n_0} \ell(f_0(x_{0,i}), \tilde{y}_{0,i})}_{\hat{R}_0^{\text{rect}}}. \quad (33)$$

We partition the unlabeled set into n_0 disjoint blocks, each containing N_0/n_0 points. The i -th labeled sample is paired with the unlabeled block $j \in [(i-1)N_0/n_0 + n_0 + 1, iN_0/n_0 + n_0]$. The block-wise estimator can be denoted as

$$\hat{R}_0^{\text{PP}} = \frac{1}{n_0} \sum_{i=1}^{n_0} \left(\frac{n_0}{N_0} \sum_{j=(i-1)\frac{N_0}{n_0}+n_0+1}^{i\frac{N_0}{n_0}+n_0} \eta_0 \cdot \ell(f_0(\tilde{x}_{0,j}), \tilde{y}_{0,j}) + \ell(f_0(x_{0,i}), y_{0,i}) - \eta_0 \cdot \ell(f_0(x_{0,i}), \tilde{y}_{0,i}) \right). \quad (34)$$

For convenience, define the per-sample risk

$$z_{0,i}^{\text{PP}} = \frac{n_0}{N_0} \sum_{j=(i-1)\frac{N_0}{n_0}+n_0+1}^{i\frac{N_0}{n_0}+n_0} \eta_0 \cdot \ell(f_0(\tilde{x}_{0,j}), \tilde{y}_{0,j}) + \ell(f_0(x_{0,i}), y_{0,i}) - \eta_0 \cdot \ell(f_0(x_{0,i}), \tilde{y}_{0,i}). \quad (35)$$

Thus, the prediction-powered estimate (17) is given by average $\hat{R}_0^{\text{PP}} = n_0^{-1} \sum_{i=1}^{n_0} z_{0,i}^{\text{PP}}$. Therefore, the upper bound can be obtained by the algorithms proposed in (Waudby-Smith & Ramdas, 2024). By viewing $z_{0,i}^{\text{PP}}$ as new data points, we can naturally call the Betting algorithm to get the required upper bound of source risk. Since \hat{R}_0^{PP} is an unbiased estimate of R_0 , the resulting bound is naturally valid.

A.3. Proof of Lemma 3.3

For a fixed $\hat{R}_{t-1}^{\text{PP}}$, we have

$$\mathbb{E}[(\hat{R}_t^{\text{PP}}(\eta_t) - \hat{R}_{t-1}^{\text{PP}})^2] = \text{Var}(\hat{R}_t^{\text{PP}}(\eta_t)) + (\mathbb{E}[\hat{R}_t^{\text{PP}}(\eta_t)] - \hat{R}_{t-1}^{\text{PP}})^2. \quad (36)$$

Using $\mathbb{E}[\hat{R}_t^{\text{PP}}(\eta_t)] = R_t$, this becomes

$$\mathbb{E}[(\hat{R}_t^{\text{PP}}(\eta_t) - \hat{R}_{t-1}^{\text{PP}})^2] = \text{Var}(\hat{R}_t^{\text{PP}}(\eta_t)) + (R_t - \hat{R}_{t-1}^{\text{PP}})^2. \quad (37)$$

The second term depends only on R_t and $\hat{R}_{t-1}^{\text{PP}}$, and is therefore independent of the tuning parameter η_t . Consequently, maximizing the expectation η_t is equivalent to minimizing the variance term $\text{Var}(\hat{R}_t^{\text{PP}}(\eta_t))$. Noting that this variance minimization problem is the same as Example 6.1 of PPI++ (Angelopoulos et al., 2023b), we thus directly have the following optimal solution:

$$\eta_t^* = \frac{\text{Cov}(u_t, \tilde{u}_t)}{(1 + \frac{n_t}{N_t}) \text{Var}(\tilde{u}_t)}. \quad (38)$$

B. Unsupervised Lower Confidence Sequences

Unsupervised risk monitoring has been recently proposed as a technique to track the performance of methods in scenarios where only an *unlabeled* test stream $\tilde{\mathcal{D}}_t = \{\tilde{x}_{t,i}\}_{i=1}^{N_t}$ is available. To address the lack of labels, the authors of (Schirmer et al., 2025) replace a sequence of supervised losses with a sequence of loss proxies that can be computed directly from the unlabeled test stream. This approach enables the derivation of an unsupervised lower bound on the running test risk, which can then be used to design an unsupervised alarm function.

The core idea is to employ a proxy function $g(\cdot)$, serving as a loss proxy for the model $f(\cdot)$, defined as $r_t = g(x_t, f)$. In addition to being unsupervised (i.e., depending only on inputs x_t), the proxy should be at least partially informative about the corresponding loss variable. When $g(\cdot)$ satisfies Assumption 1 in (Schirmer et al., 2025), Assumption 1. Given a sequence of losses $r_{0:t}$, let the corresponding sequence of loss proxies $u_{0:t}$ and proxy thresholds $\beta_0, \dots, \beta_t \in \mathbb{R}$, along with a loss threshold τ , be such that for all $t \geq 1$, the following inequality holds:

$$\frac{1}{t} \sum_{t'=1}^t \underbrace{\mathbb{P}_{P_{t'}}(r_{t'} > \beta_{t'}, r_{t'} \leq \tau)}_{\text{PFP}_{t'}} \leq \underbrace{\mathbb{P}_{P_0}(r_0 > \beta_0, u_0 \leq \tau)}_{\text{PFP}_0} + \frac{1}{t} \sum_{t'=1}^t \underbrace{\mathbb{P}_{P_{t'}}(r_{t'} \leq \beta_{t'}, u_{t'} > \tau)}_{\text{PFN}_{t'}}. \quad (39)$$

The running test risk can be lower bounded as

$$\bar{R}_t(p_{1:t}) \geq \tau \left(\frac{1}{t} \sum_{t'=1}^t \mathbb{P}_{P_{t'}}(r_{t'} > \beta_{t'}) - \mathbb{P}_{P_0}(r_0 > \beta_0, u_0 \leq \tau) \right), \quad \forall t \geq 1. \quad (40)$$

Specifically, the authors of (Schirmer et al., 2025) proposed online threshold calibration to select $\beta_0, \dots, \beta_t \in \mathbb{R}$ and τ by maximizing the F1 score based on the source model's proxy. Importantly, this bound depends only on the test loss proxies and the source loss, which means that its corresponding lower-bound confidence sequence can be evaluated using a combination of unlabeled test data $\{\tilde{\mathcal{D}}_{t'}\}_{t'=1}^t = \{\{x_{t',i}\}_{i=1}^{N_{t'}}\}_{t'=1}^t$ and labeled source data $\tilde{\mathcal{D}}_0$. In practice, this requires computing an empirical estimate of $\mathbb{P}_{P_{t'}}(r_{t'} > \beta_{t'})$ at each step, followed by the construction of a lower confidence sequence relying on specific bounds. This makes it suitable for the final proposed unsupervised alarm:

$$\Phi_t^b = \mathbb{1}[L_t(r_{0:t}, \beta_{0:t}, u_0, \tau) > U_0(r_0) + \epsilon_{\text{tol}}]. \quad (41)$$

C. Additional Experiments

C.1. Sequential Risk Monitoring on Image Data

In Figure 5(a), we evaluate image classification risk under increasing distribution shift severity, using the squared loss. We observe a consistent performance gain achieved by PPRM. In Figure 5(b), we further consider non-monotonic distribution shift scenarios, where PPRM continues to outperform all benchmark methods.

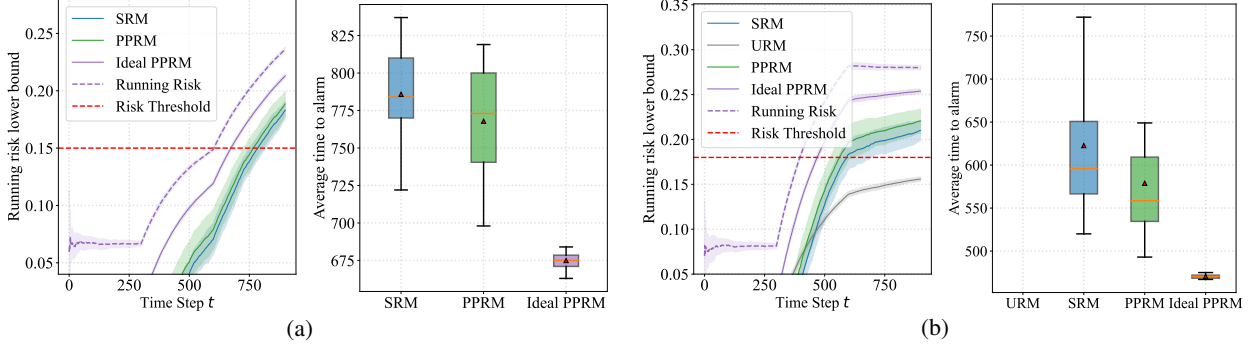


Figure 5. Risk estimates as a function of time t and average time to alarm for an image classification task: (a) under increasing shift severity (squared loss); (b) under a non-monotonic shift severity (binary loss).

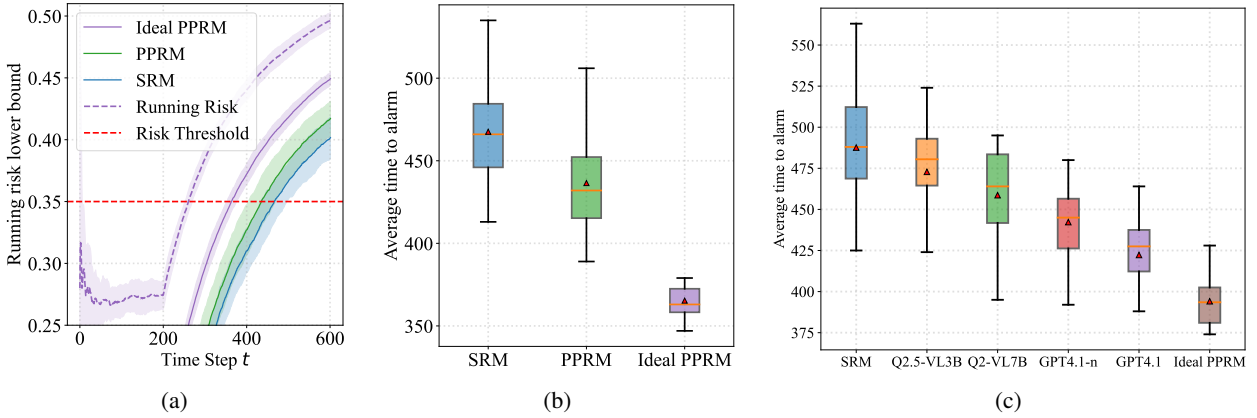


Figure 6. Performance for the LLM QA task under prompt shifts: (a) running risk lower bounds; (b) average time to alarm; (c) average time to alarm using different predictors.

C.2. Monitoring an LLM with Limited Human-Labeled Data

In Figure 6, we report additional results for monitoring another lightweight model: the 4-bit quantized version of MedGemma-4B-IT (Sellergren et al., 2025), which is specialized for the medical domain. For the predictor $f_p(\cdot)$, we employ the non-specialized model, Qwen2.5-VL-7B. The evaluation begins with medical questions and gradually incorporates queries from another domain. The results are consistent with those presented in the main text, demonstrating the generalization capability of PPRM.

C.3. Detecting the Need for Channel Covariance Re-Estimation

In wireless communication, reliable communication depends on accurate knowledge of the channel statistics, particularly the channel covariance matrix that determines both the quality of *minimum mean-square error* (MMSE) estimation and the performance of downstream decoders. However, in practical wireless systems, the propagation environment evolves over time due to user mobility and temporal variations in interference. These drifts cause a mismatch between the true channel distribution and the one assumed by the receiver, leading to degraded channel estimates and increased decoding errors. As a result, a central question is when the receiver should trigger covariance re-estimation or retraining of its model parameters. Re-estimating too frequently wastes pilot and computation resources, whereas re-estimating too late leads to significant performance loss. This motivates a principled mechanism that can continuously monitor the channel quality and reliably detect when a statistically significant covariance shift occurs. In this subsection, we examine a communication-inspired setting where the monitored model operates over a channel whose characteristics may drift over time.

C.3.1. PROBLEM FORMULATION

We consider a standard uplink communication scenario with a *base station* (BS) equipped with M antennas and a single-antenna *user equipment* (UE). We assume block flat-fading channels, where each coherence block contains τ_c complex-valued samples. We denote by t the index associated with a single coherence block. Each block contains n_f frames for data transmission, with each frame consisting of a codeword encoding a different message. For each frame i in a coherence block t , the $M \times 1$ received signal at the BS is given by $v_t[i, j] = h_t s_t[i, j] + e_t[i, j]$, $j = 1, \dots, n_w$, where n_w is the codeword length, $s_t[i, j] \in \mathbb{C}$ is the information-bearing signal transmitted over channel use j , which is drawn from an existing constellation \mathcal{M} , h_t is the $M \times 1$ channel vector, and $e_t[i, j] \sim \mathcal{CN}(0, \sigma^2 I_M)$ represents *additive white Gaussian noise* (AWGN) with zero mean and covariance $\sigma^2 I_M$.

The channel vectors are assumed to be conditionally Gaussian distributed given a set of parameters ψ_t , i.e., $h_t | \psi_t \sim \mathcal{CN}(0, C(\psi_t))$. The parameter ψ_t accounts for geometric and electromagnetic properties of the propagation environment that change slowly over the coherence interval index t . Furthermore, the covariance matrix can be expressed as

$$C_t = C(\psi_t) = \int_{-\pi}^{\pi} g(\theta_t; \psi_t) a(\theta_t) a^H(\theta_t) d\theta_t, \quad (42)$$

where $g(\theta_t; \psi_t) \geq 0$ is the power density function dictated by the parameters ψ_t and $a(\theta_t)$ denotes the array response vector at the BS for an angle of arrival θ_t .

In order to support the estimation of the channel covariance matrix C_0 and the channel noise σ^2 , at the first coherence block, indexed as $t = 0$, the UE sends $n_c \leq \tau_c$ pilots $x_c = [x_c[1], \dots, x_c[n_c]]^\top \in \mathbb{C}^{n_c \times 1}$. In order to estimate the parameters C_0 and σ^2 , we adopt the positive semidefinite least squares estimate approach introduced in (Dietrich et al., 2006), and the estimated parameters are represented by \hat{C}_0 and $\hat{\sigma}^2$.

At each coherence block t , excluding $t = 0$, n_h pilots $x_{t,h} = [x_{t,h}[1], x_{t,h}[2], \dots, x_{t,h}[n_h]]^\top \in \mathbb{C}^{n_h \times 1}$ are transmitted to enable channel estimation. We consider MMSE channel estimation, and thus the estimated channel vector \hat{h}_t is given by

$$\hat{h}_t = \hat{C}_0 Z_{t,h}^H \left(Z_{t,h} \hat{C}_0 Z_{t,h}^H + \hat{\sigma}^2 I_{Mn_h} \right)^{-1} y_{t,h}, \quad (43)$$

where $Z_{t,h} = x_{t,h} \otimes I_M$ and $y_{t,h} = Z_{t,h} h_t + e_{t,h}$. At each block t , the BS carries out equalization using the estimated channel vector \hat{h}_t in (43). The MMSE equalized signal $\tilde{s}_t[i, j]$ is obtained as $\tilde{s}_t[i, j] = (\hat{h}_t^H \hat{h}_t + \hat{\sigma}^2)^{-1} \hat{h}_t^H v_t[i, j]$. The equalized symbols for each frame are processed by an NN-based decoder, $f(\cdot)$, to obtain an estimate of the transmitted codeword, $\hat{s}_t[i, j] = \arg \max_{m \in \mathcal{M}} f(\tilde{s}_t[i, j])_m$, where \mathcal{M} denotes the modulation set. For risk monitoring, we additionally introduce n_r pilots, $x_{t,r} = [x_{t,r}[1], x_{t,r}[2], \dots, x_{t,r}[n_r]]^\top \in \mathbb{C}^{n_r \times 1}$. The equalized pilots signal is denoted as $\tilde{x}_{t,r} = [\tilde{x}_{t,r}[1], \tilde{x}_{t,r}[2], \dots, \tilde{x}_{t,r}[n_r]]^\top \in \mathbb{C}^{n_r \times 1}$. These signals are decoded by the decoder, and the decoded pilots are denoted as $\hat{x}_{t,r} = [\hat{x}_{t,r}[1], \hat{x}_{t,r}[2], \dots, \hat{x}_{t,r}[n_r]]^\top \in \mathbb{C}^{n_r \times 1}$.

At each coherence block $t \geq 1$, we collect two sets of observations:

- A labeled set from additional pilot symbols: $\mathcal{D}_t = \{(\tilde{x}_{t,r}[k], x_{t,r}[k]) \mid k = 1, \dots, n_r\}$, where $x_{t,r}[k]$ is the ground-truth transmitted pilot symbol.
- An unlabeled set from data symbols: $\tilde{\mathcal{D}}_t = \{\tilde{s}_t[i, j] \mid i = 1, \dots, n_f, j = 1, \dots, n_w\}$, for which the true symbol $s_t[i, j]$ is unknown.

Given a decoder $f(\cdot)$ producing the symbol estimate $\hat{s}_t[i, j] = \arg \max_{m \in \mathcal{M}} f(\tilde{s}_t[i, j])_m$, the prediction-powered risk estimator at block t is given by

$$\hat{R}_t^{\text{PP}} = \underbrace{\frac{\eta_t}{n_w n_f} \sum_{i=1}^{n_f} \sum_{j=1}^{n_w} \ell(f(\tilde{s}_t[i, j]), \hat{s}_t[i, j])}_{\hat{R}_t^{\text{U}}} + \underbrace{\frac{1}{n_r} \sum_{k=1}^{n_r} \left(\ell(f(\tilde{x}_{t,r}[k]), x_{t,r}[k]) - \eta_t \cdot \ell(f(\tilde{x}_{t,r}[k]), \hat{x}_{t,r}[k]) \right)}_{\hat{R}_t^{\text{rect}}}. \quad (44)$$

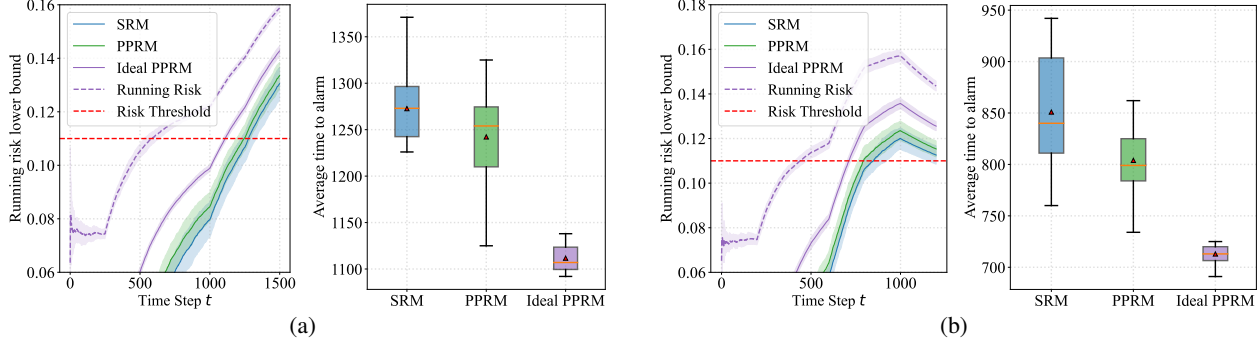


Figure 7. Risk estimates as a function of time t and average time to alarm for the channel equalization task: (a) under increasing ψ_t ; (b) under a non-monotonic ψ_t .

C.3.2. RESULTS

We consider a scenario for the simulation in which a BS with 16 antennas receives uplink transmissions from a single-antenna UE. The BS antenna array is assumed to be a uniform linear array, with an inter-element spacing of half the wavelength. The codeword length is set to $n_w = 16$, the number of frames per coherence block is $n_f = 2$ and the signal-to-noise ratio is $\rho/\sigma^2 = 6$ dB. Additionally, we set $n_c = 500$, $n_h = 3$, and, $n_r = 1$. For simplicity, we consider the 3GPP spatial channel model for a uniform linear array with only a single propagation path. In this case, we have only one parameter for the covariance matrix: the angle of the path center $\delta_t \in [-\pi/2, \pi/2]$, which is uniformly distributed. The power density function of the angle of arrival is given by the Laplace density

$$g(\theta_t; \psi_t) = \exp\left(-\frac{d_{2\pi}(\theta_t, \psi_t)}{\sigma_{\text{ASD}}}\right), \quad (45)$$

where $d_{2\pi}(\theta_t, \psi_t)$ is the wrap-around distance between θ_t and ψ_t , which can be thought of as $|\theta_t - \psi_t|$ for most (θ_t, ψ_t) pairs. In addition, σ_{ASD} is the angular standard deviation, as it determines how large the deviations from the nominal angle are. We gradually change the parameter ψ_t to simulate the increase of risk. Besides, squared loss is selected as the risk function.

Here we investigate a self-synthetic setting, where no additional models are needed to generate the synthetic labels. The results in Figure 7 demonstrates that PPRM can achieve earlier detection on average compared to SRM. These results highlight PPRM's suitability for on-device model maintenance, where quick adaptation decisions are critical under bandwidth and labeling constraints.